

Entanglement cones and horizons in analogue cosmological production of Dirac fermions

C. Fulgado-Claudio^{1,*} and A. Bermudez¹

¹*Instituto de Física Teórica, UAM-CSIC, Universidad Autónoma de Madrid, Cantoblanco, 28049 Madrid, Spain.*

Although gravitational particle production in curved quantum field theories (cQFTs) is key to our understanding of the early universe and black hole physics, its direct observation requires extreme conditions or unrealistic sensitivities. Recent progress in quantum simulators indicates that analogues of gravitational particle production can be observed in table-top experiments of cold atomic gases described by effective cQFTs. This promises a high degree of tunability in the synthesised curved spacetimes and, moreover, sets a clear roadmap to explore the interplay of gravitational particle production with other non-perturbative effects genuine to interacting QFTs. We hereby focus on the appearance of fermion condensates for self-interacting Dirac fermions, and study how dynamical mass generation and spontaneous symmetry breaking affects real-time dynamics. We use the entanglement contour as a tool to analyze the spatio-temporal causal structure of particle production, showing how it can account for the cosmological horizon in accelerating spacetimes, while also being sensitive to the effect of different symmetry-breaking processes. In particular, we show that the combined breakdown of time-reversal symmetry due to the expanding spacetime, and parity due to a pseudo-scalar condensate, manifest through the structure of the light-cone-like propagation of entanglement in this analogue cQFT.

Introduction.— Quantum simulators (Qs) promise to become a transformative tool to explore the complex quantum many-body frontier common to various disciplines of contemporary science [1–3]. In theoretical physics, Qs can sometimes realize analogues of phenomena that would otherwise be difficult to observe, if not altogether impossible, in their original realm. These two aspects come together in the study of quantum field theories (QFTs) in curved spacetimes [4–10] by means of experimental quantum devices [11–16] that can be used to explore foundational questions about gravity, or test our current cosmological models of the universe. These Qs foster a genuinely multidisciplinary approach that integrates concepts from atomic physics, quantum optics and quantum information theory, with those of high-energy physics and general relativity. A particularly-relevant example is that of quantum entanglement [17–19], which provides insights into the role of quantum correlations in the complexity frontier of many-body systems, and plays an important role in questions as diverse as the nature of the QFT vacuum or the evaporation of black holes, and also possibly in the information paradox for the structure of spacetime at the quantum level.

In this Letter, we focus on Qs of ultra-cold atoms in Raman optical lattices [20–27] as analogues of particle production of self-interacting Dirac fermions in an effective spacetime with a tunable accelerated expansion. We demonstrate how the entanglement contour [28], when combined with a non-perturbative variational ansatz based on fermionic Gaussian states [29, 30], can provide a clean spatio-temporal resolution for the real-time dynamics of these Dirac fields. Looking at particle production through this entanglement-contour lens, we unveil interesting phenomena like a cosmological particle horizon in the entanglement spreading, and the impact on the entanglement-cone structure of symmetry-breaking fermion condensates during particle production, pointing at future research opportunities in analogue gravity [31].

The model. We consider a Friedmann-Robertson-Walker spacetime $ds^2 = dt^2 - a^2(t)d\Sigma^2$ with a scale factor $a(t)$. In a cosmological scenario [32], the scale factor connects an in-

flationary epoch to our current dark-energy and dark-matter dominated universe in $D = 3 + 1$ dimensions. In contrast, in an analogue setup, we are free from these constraints, and can: (i) connect two asymptotic Minkowski regions $a_0 \rightarrow a_f$ by an exponential scale factor controlled by the Hubble rate H , such that the duration is $\Delta t = \frac{1}{H} \log \frac{a_f}{a_0}$; (ii) vary the Hubble rate at will, as it is not fixed by cosmological observations, interpolating between adiabatic $H \rightarrow 0$ and sudden $H \rightarrow \infty$ expansions; and (iii) explore reduced dimensionalities that may lead to simpler analogue experiments. This flexibility extends to the (iv) dynamical quantum fields that fill in this expanding spacetime which, in the standard cosmological model of inflation, correspond to a scalar field under certain self-interaction potentials. For the reasons exposed below, we shall be interested instead in self-interacting Dirac spinors $\hat{\psi}(x) \rightarrow \hat{\psi}_i(t)$ discretized on a co-moving chain $x_i = ia$, where a is the lattice spacing and $i \in \mathbb{Z}_{N_s}$. By using conformal time via $\eta = \int dt/a(t)$, and rescaling the fields as $\hat{\psi}_i \rightarrow \sqrt{a(\eta)}\hat{\psi}_i$, there is not need to simulate an inflating lattice with increasing proper distance $d_{ij}(t) = a(t)|x_i - x_j|$, and the regularised action reduces to a fermionic QFT with explicit dependence on conformal time. Finally, we can also (iv) explore the subsequent evolution of the produced particles within a flat spacetime a_f , which will allow us to derive a neat picture of thermalization as these particles fill in the universe.

We work with a Hamiltonian lattice field theory with rescaled spinors and conformal time associated to the original cQFT action that includes vierbein fields and the spin connection [33]. In particular, we employ a Wilson-type regularization to deal with fermion doubling [34] which, in momentum space, yields a free part $\hat{H} = \sum_{k \in \text{BZ}} \hat{\psi}_k^\dagger h_k(ma(\eta)) \hat{\psi}_k$ with

$$h_k(ma(\eta)) = -\frac{\sin ka}{a} \gamma^0 \gamma^1 + \left(ma(\eta) + \frac{1 - \cos ka}{a} \right) \gamma^0, \quad (1)$$

where the matrices are $\gamma^0 = \sigma^z$, $\gamma^1 = i\sigma^y$ and $\gamma^5 = \gamma^0 \gamma^1$. This free field theory has a simple interpretation as a tight-binding model on a synthetic ladder, and can be realised with minor modifications of recent experiments with alkaline atoms in op-

tical Raman lattices [27]. Here, the ladder legs represent the spinor components, encoded in two hyperfine levels of ^{87}Sr , and an energy imbalance that accounts for the time-dependent mass $ma(\eta)$ can be controlled by the Raman lasers detuning.

Being quadratic, Wick's theorem holds for this part, and the real-time dynamics can be fully characterised through the correlation matrix $\Gamma_{ij}(\eta) = \langle \psi(\eta) | \hat{\psi}_i \hat{\psi}_j^\dagger | \psi(\eta) \rangle$. Regarding the full many-body Hilbert space, the dynamics is constrained to a reduced manifold of so-called fermionic Gaussian states (fGS) $\{|\psi(\Gamma)\rangle : \Gamma \in \text{GL}_{4N_s}(\mathbb{C})\}$ during the expansion. This can then be used as a variational family to approximate genuinely-interacting QFTs. In this limit, particle production [4, 5] can be formalised by a Bogoliubov transformation [35, 36] that acts by mapping $|\psi(\Gamma_0)\rangle \mapsto |\psi(\Gamma_f)\rangle$ producing particles. Taking advantage of the above points (i)-(iv), we can actually go beyond this simple limit and explore non-perturbative effects by including self-interactions according to the Gross-Neveu model [37], namely

$$\hat{V}_{\text{int}} = \frac{g_0^2}{2} \sum_i \left(\hat{\psi}_i^\dagger \gamma^0 \hat{\psi}_i \right)^2, \quad (2)$$

where g_0^2 is the dimensionless coupling strength which, in contrast to the bare mass, does not get renormalised by the scale factor. In a previous work [38], we have indeed shown that the fGS ansatz can be used to approximate the vacuum $|\psi(\Gamma_0)\rangle$, and that it coincides exactly with large- N predictions [39]. The fGS predictions account for the onset of scalar and pseudo-scalar fermion condensates, which are specific elements of the correlation matrix of fermion bilinears $\Sigma = g_0^2 \sum_k \langle \hat{\psi}_k^\dagger \gamma^0 \hat{\psi}_k \rangle / 2aN_s$, $\Pi = ig_0^2 \sum_k \langle \hat{\psi}_k^\dagger \gamma^1 \hat{\psi}_k \rangle / 2aN_s$. During the expansion, these condensates will evolve non-perturbatively affecting the particle production and vice versa, which we can approximate variationally via our fGS, leading to a set of self-consistent non-linear differential equations

$$i \frac{d}{d\eta} \Gamma(\eta) = [\tilde{h}_k(ma(\eta), \Gamma(\eta)), \Gamma(\eta)], \quad (3)$$

where $h_k \rightarrow \tilde{h}_k(ma(\eta), \Gamma) = h_k(ma(\eta) + \Sigma(\Gamma)) - i\Pi(\Gamma)\gamma^1$. We see how the non-linearities arise through \tilde{h}_k via the self-energy expressed in terms of the condensates, which follows from Wick's theorem on the fGS manifold $\langle \psi(\Gamma) | \hat{V}_{\text{int}} | \psi(\Gamma) \rangle$.

Solving these equations with the initial condition $|\psi(\Gamma_0)\rangle$ one obtains a time-evolved fGS $|\psi(\Gamma(\eta_f))\rangle$ with a non-vanishing density of particles with respect to the instantaneous groundstate $|\psi(\Gamma_f)\rangle$ at (ma_f, g_0^2) . Within our variational approximation, the interpretation in terms of a Bogoliubov transformation is still useful, but it now depends on the full non-perturbative time history $\{\Gamma\}_\eta = \{\Gamma(\eta) : \eta \in [\eta_0, \eta_f]\}$, allowing to express the evolved state as

$$|\psi(\Gamma(\eta_f))\rangle = \bigotimes_{k \in \text{BZ}} \left(\alpha_k(\{\Gamma\}_\eta) - \beta_k(\{\Gamma\}_\eta) a_k^\dagger b_{-k}^\dagger \right) |0\rangle, \quad (4)$$

with normalised Bogoliubov parameters $|\alpha_k|^2 + |\beta_k|^2 = 1$. The density of produced fermions after the expansion is $n_a =$

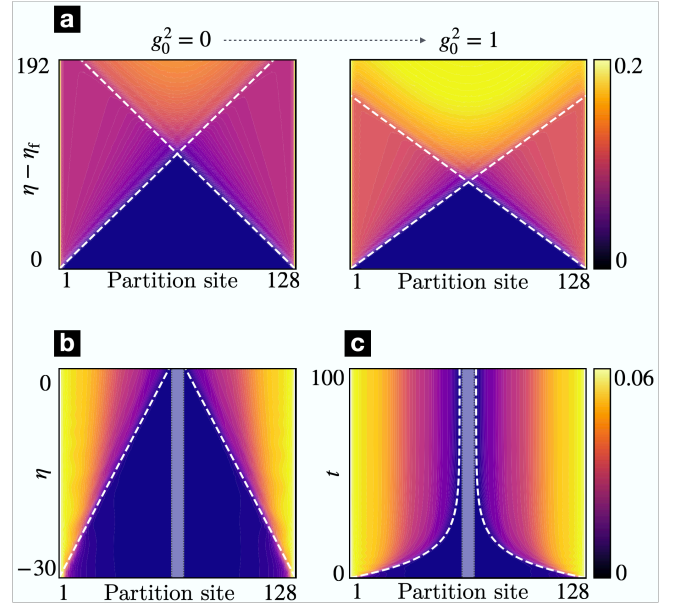


FIG. 1. (a) Spatio-temporal propagation of EC in the asymptotic flat region a_f , both in the free $g_0^2 = 0$ and in the interacting $g_0^2 = 1$ regimes, and setting $ma = -1$, $a_0 = 0.7$, $a_f = 1.3$, $Ha = 100$ (sudden expansion). The dashed white lines indicate the light-cone-like predictions based on the group velocity after the sudden expansion. (b,c) Spatio-temporal propagation of EC during a de Sitter expansion, using conformal and cosmological time respectively, and setting $ma = 1$, $Ha = 0.1$, $g_0^2 = 2$, $a_0 = 1/3$, with η and t expressed in lattice units. The expansion in (b) starts at $\eta_0 a = -30$ and extends to the distant future $\eta \rightarrow 0^-$, approximated by $\eta a = -0.001362$. The shaded regions denote the asymptotic spatial boundary that particles cannot cross. In (c) the corresponding expansion covers $t_0 = 0$ to $ta \rightarrow \infty$, here approximated by $t = 100/a$.

$n_b = \sum_{k \in \text{BZ}} |\beta_k(\{\Gamma\}_\eta)|^2 / aN_s a_f$, which is the result of a back-to-back production of particle-antiparticle pairs. We note that previous works [40–43] on free QFTs have exploited the formal analogy of this transformation with two-mode squeezing to characterise mode entanglement in a cosmological scenario in momentum space, here connected to entanglement between right- and left-moving excitations. This, however, does not provide any spatial resolution that links to the causal propagation of entanglement, or to the existence of cosmological horizons due to an accelerated expansion. Moreover, to our knowledge, there has been no prior study of the effect of interactions and fermion condensates on the entanglement during gravitational expansion. We fill in both gaps in this work.

Correlation light cones.— Let us start moving away from the aforementioned mode entanglement by focusing on the block entanglement entropy (EE) $S_A = -\text{Tr}(\rho_A \log \rho_A)$, which quantifies the amount of quantum correlations across the AB bipartition of the system $\rho_A = \text{Tr}_B |\psi\rangle\langle\psi|$, where A would be a block of ℓ_A sites. We note that the EE has been studied in great detail for quantum quenches in many-body models, where a system evolves under a sudden change of the Hamiltonian, yielding a neat quasi-particle picture in which a linear

entanglement growth is a manifestation of a light-cone-like propagation of excitations [44–50].

Given that the Hubble rate H allows us to smoothly interpolate between sudden and adiabatic limits, it is very natural to extend this EE quasi-particle picture to our cosmological scenario. Moreover, resorting to the concept of entanglement contour (EC) [28], which assigns to each site i of the partition a specific contribution S_i to the overall EE, such that $\sum_i S_i = S_A$, one can get further information on the local distribution of entanglement within the block, allowing us to bring this quasi-particle picture to a new domain. In particular, we show below that the EC allows identifying a cosmological particle horizon due to the accelerating spacetime. Although a general recipe for the calculation of EC in generic setups is lacking, the fGS ansatz provides a well-defined approximation to the EC via the aforementioned correlation matrix $\Gamma(\eta)$, as the spectrum of the block density matrix ρ_A is determined by the restricted correlation matrix $(\Gamma_A(\eta))_{ij} = \Gamma_{ij}(\eta)|_{i,j \in A}$ [51, 52]. Diagonalizing this matrix by a unitary transformation $U^\dagger \Gamma_A U = \text{diag}(\{v_k\}_{k \in \text{BZ}})$, the EC $S_i(\eta) = \sum_{k \in \text{BZ}} p_i(k, \eta) s_k(\eta)$ weighs each contribution $s_k(\eta) = -v_k(\eta) \log v_k(\eta) - (1 - v_k(\eta)) \log(1 - v_k(\eta))$ at the i -th site by $p_i(k, \eta) = |U_{ki}(\eta)|^2$. Since this matrix is determined self-consistently (3), we can explore how entanglement evolves in the spacetime coordinates under interaction effects beyond perturbation theory, e.g. symmetry breaking. Let us start by studying how the particles created during the expansion propagate in the asymptotically-flat out region a_f , where the conformal time becomes linearly related to the cosmological time $\eta = \eta_f + (t - t_f)/a_f$ and can attain arbitrarily-large values. In Fig. 1(a), we depict the spatiotemporal EC profile for a partition of $\ell_A = 128$ sites in a $N_S = 512$ lattice in real time. In the free case $g_0^2 = 0$, one observes a clear light-cone-like propagation of entanglement. In the scaling limit, $\ell_A, t \rightarrow \infty$ with t/ℓ_A finite, this propagation of EC can be obtained by extending the EE quasi-particle picture to the EC, as discussed in the Supplemental Material [53]. The cones emanate from the block boundaries, separating causally connected and disconnected spacetime regions, and show a slope that is set by twice the group velocity $v_g = \max_{k \in \text{BZ}} |\partial_k \epsilon_k|$, where ϵ_k is the energy of a particle or antiparticle obtained by diagonalising h_k (1). Interestingly, this picture predicts that the entanglement equilibrates and there is an equipartition across the block $S_i(\eta) = S_0 \forall i \in A$, such that the EE fulfills a volume law that agrees with the eigenstate thermalization hypothesis [54–56] and a generalised Gibbs ensemble (GGE) that approximates ρ_A [57].

When we switch on interactions to $g_0^2 = 1$, the scalar condensate attains a non-zero value in the initial state and displays a non-trivial time evolution $\Sigma(\eta)$. This results in a new dispersion relation from Eq. (3) that is corrected by a time-dependent self-energy and can, consequently, lead to a dynamical group velocity $v_g(\eta)$. In this case, the previous conserved quantities associated to the GGE become time-dependent, and may compromise the validity of the quasi-particle prediction. However, for certain regimes in which the

condensate relaxes to a certain value, one expects to be able to derive a hydrodynamic description for the EC by renormalising the spread velocity and the particle-antiparticle mode entanglement. We confirm this expectation in the right panel of Fig. 1(a), where we show that the EC light cones follow $x(\eta) \approx \pm 2v_g^{\text{int}}\eta$, where v_g^{int} is a renormalised velocity. As shown in the figure, the cones get tilted with respect to $g_0^2 = 0$, showing that this propagation speed is enhanced by interactions. Although this is counterintuitive at first, as the continuum QFT predicts a dynamical mass generation that would slow the dynamics of excitations, the problem on the lattice is richer as this dynamically-generated mass can bring one closer or further apart from a critical line around which the continuum limit should be valid. In this case, increasing interactions brings us closer, reducing the gap and also the overall bare mass, such that the particle-anti-particle pairs propagate faster. Let us emphasise that this renormalised quasi-particle picture can actually be completely broken for stronger interactions in which the pseudo-scalar condensate is also non-vanishing $\Pi(\eta)$. We find in that case that the group velocity develops persistent oscillations that make a quasi-particle prediction very inaccurate EC (see the Supplemental Material [53]).

Correlation horizons.— Let us now turn to a key phenomenon that becomes apparent via the EC dynamics during the accelerated de Sitter expansion $a(\eta)$, and after it as above. For this cosmological expansion, a particle horizon determines when the distance between the emission of a particle and its subsequent detection starts to expand faster than the speed of light. Accordingly, spacetime breaks in causally disconnected regions that can have no influence on one another and, thus, no entanglement. In conformal time, the appearance of this horizon in the EC is a bit subtle. In Fig. 1(b) we show the evolution of EC during the expansion, which shows a ballistic spread as before, but this time is upper bounded by $\eta = 0$, as cosmological time squeezes in the distant future as a result of the exponential scale factor [58].

In Fig. 1(c), we show the EC profile in cosmological time t , which clearly shows how the propagation cones get curved as a consequence of the expansion of the universe, leading to a pair of asymptotes that separate regions that cannot be causally connected. We see two separated spatial regions where entanglement attains non-vanishing values as time elapses but, due to the accelerated expansion, these are separated by a finite region with a width $\Delta x = \ell_A - \frac{4v_g}{H a_0}$ in which the EC is always vanishing. We emphasize that the spatial resolution brought by the EC as opposed to the EE is crucial to identify these correlation horizons. It is also interesting to note that the EC distribution within the causally-connected parts does not fulfill an equipartition, so the evolution in this case is very different from an equilibration to a GGE. Had we let the system evolve in the Minkowski out region a_f , the particle-anti-particle pairs would have had sufficient time to propagate in this static background, such that the causally-disconnected regions would again be connected

by subsequent correlation cones as before, leading to volume-law entanglement and GGE.

Symmetry breaking in the entanglement contour.— We have previously mentioned in passing that expansions in which the pseudo-scalar condensate is non-vanishing $\Pi(\eta)$ can have a bigger impact on the spread of entanglement. We now explore this further, considering that parity gets spontaneously broken, which will impact the properties of the EC under point-like transformations [28]. Specifically, the EC satisfies that $S_i = S_j$ if the system is invariant under a transformation that exchanges two sites, $\hat{U}_{ij}\hat{\psi}_i\hat{U}_{ij}^{-1} = e^{i\xi}\hat{\psi}_j$, where $\xi \in \mathbb{R}$ and $i \neq j$. To understand this property better, we temporarily focus on the discrete symmetries of the static model $a(\eta) = 1$, which connects to the tenfold classification of topological insulators [59–61]. For $\Pi = 0$, the system is invariant under time-reversal \hat{T} and particle-hole \hat{C} transformations, as well as their combination $\hat{S} = \hat{T}\hat{C}$. At the single-particle level, these transformations are realised by $T = T\mathcal{K}$ with $T = \gamma^0$, $C = C\mathcal{K}$ with $C = \gamma^0\gamma^1$, and $S = \gamma^0\gamma^5$, where \mathcal{K} denotes complex conjugation such that $T^\dagger h_{-k}^* T = h_k$, $C^\dagger h_{-k}^* C = -h_k$ and $S^\dagger h_k S = -h_k$. These operators satisfy $T^2 = C^2 = S^2 = 1$. In addition, parity symmetry \hat{P} is realised as $P = \gamma^0$ such that $P^\dagger h_{-k} P = h_k$. Indeed, together with translational invariance, parity symmetry describes the invariance under a mirror symmetry about any point and, in particular, about the center of the A block, which leads to a site exchange \hat{U}_{ij} with $j = \ell_A + 1 - i$. According to our previous comment, if parity is conserved, one expects the EC to display the symmetry $S_i = S_{\ell_A+1-i}$, which agrees with the EC cones of Fig. 1.

This situation changes when $\Pi \neq 0$, as one finds that \hat{T} is preserved, but \hat{P} , \hat{C} and \hat{S} get broken. Moreover, switching back to $a(\eta) \neq 1$ will also break \hat{T} , endowing the condensate with its own dynamics $\Pi(\eta)$, which shall affect the EC spreading as we now discuss. In the left panel Fig. 2(a), we depict the spread of the EC in complete analogy to Fig. 1, but for an expansion with a non-zero $\Pi(\eta)$. We note that in all of the case above, the ECs displayed actually correspond to one of the spinor components, namely $S_i^u(\eta)$, which does not compromise the generality as $S_i^d(\eta) = S_i^u(\eta) =: S_i(\eta)$. This no longer holds when $\Pi(\eta) \neq 0$, and one can observe in the right panel of Fig. 2(a) that the EC for the down spinor $S_i^d(\eta)$ is indeed different, with a larger spread of entanglement from the left boundary with respect to the right one, opposite to what happens for $S_i^u(\eta)$. These figures suggest that the EC profiles are still symmetric by simultaneously exchanging left-right boundaries and up-down spinors, yielding $S_i^u(\eta) = S_{\ell_A+1-i}^d(\eta)$ and viceversa $S_i^d(\eta) = S_{\ell_A+1-i}^u(\eta)$. In fact, one can check that this is indeed a remnant symmetry that combines both parity \hat{P} and particle-hole \hat{C} symmetries $(\gamma^1)^\dagger h_k^* \gamma^1 = -h_k$, which still holds even if the individual symmetries are broken. The CP symmetry that survives a non-zero $\Pi(\eta)$ suggests that one can define a zigzag ordering of the spatial sites and spinor components and depict the site- and spinor-resolved EC as shown in Fig. 2(b). This symmetry-aware representation allows to recover a clear light-cone-like

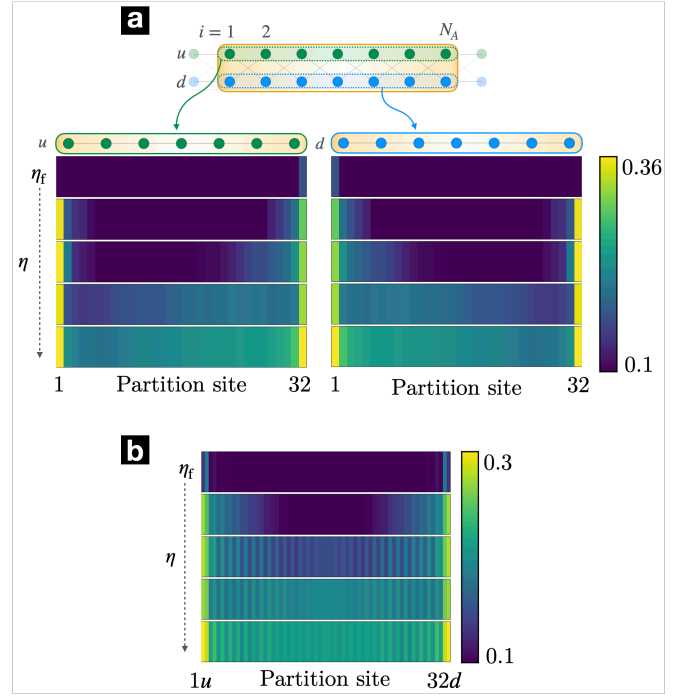


FIG. 2. Time evolution of EC for different phases for a partition A of $N_A = 32$ sites, from a system of $N_S = 128$ sites. (a) Numerical time evolution of EC for each leg of the ladder, for an expansion with $\Pi \neq 0$, with $ma = -1$, $g^2 = 0$, $a_0 = 0.7$, $a_f = 1.3$, $H = 100$ (quench limit). (b) Numerical time evolution of EC, with all the sites shown in the horizontal axis, alternating up and down spinors, for an expansion with $\Pi \neq 0$, with $ma = -1$, $g^2 = 0$, $a_0 = 0.7$, $a_f = 1.3$, $H = 100$ (quench limit).

structure characteristic of causality and connecting with the aforementioned quasi-particle picture, even in presence of a pseudo-scalar condensate and for any Hubble rate H .

This situation contrasts the dependence on H of other more standard quantities in cQFTs, such as the spectrum $|\beta_k|^2$ of produced particles $n_a \sim \int dk |\beta_k|^2 / 2\pi$. In general, the breakdown of parity translates into an asymmetric spectrum $|\beta_k|^2 \neq |\beta_{-k}|^2$, which is natural in light of its effect $\hat{\psi}_k \rightarrow \hat{P}\hat{\psi}_k\hat{P}^{-1} = \gamma^0\hat{\psi}_{-k}$. However, as shown in Fig. 3, this is only manifested at intermediate values of the Hubble rate H in accordance with our previous results [38], but a symmetric spectrum around $k = 0$ is recovered as one approaches the quench limit (see the darker blue curve). In the Supplemental Material [53], we indeed show how this peculiarity can be understood from the interplay of parity with the above discrete symmetries, applied to the instantaneous state after the sudden quench. We unveil an additional underlying symmetry that protects an equal particle production in modes k and $-k$ regardless of the breaking of parity that depends on the adiabaticity parameter H , as it is only present in the quench limit and not for slower expansions.

Conclusions and outlook.— Our study highlights the potential for observing exotic analogues of gravitational particle production in effective cQFTs that go beyond the standard cosmological model. The possibility of tuning the dimen-

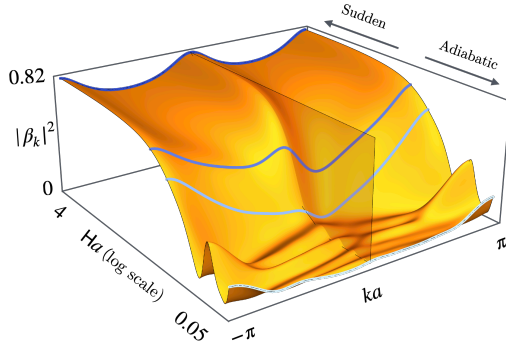


FIG. 3. Spectra of particle production for various adiabaticity regimes. The parameters are set as $ma = -1$, $g_0^2 = 3$, $a_0 = 0.7$, $a_f = 1.3$, for a chain of $N_s = 128$ sites. We highlight four values of $Ha = 4, 0.3, 0.2$ and 0.05 for increasingly lighter blue, for which the relation between symmetry of the spectrum and Ha is manifest.

sionality, designing the expansion scale factor, and tailoring the matter content of the cQFT brings a wide and largely-uncharted territory that can be addressed from a multidisciplinary viewpoint. In this work, we have focused on self-interacting Dirac QFTs in a reduced Friedman-Robertson-Walker spacetime, which have allowed us to explore how the typical phenomenon of particle-antiparticle production is affected by non-perturbative effects such as dynamical mass generation and the appearance of symmetry-broken fermion condensates. Exploiting a multidisciplinary perspective, we have analyzed this analogue cosmological setup through the lens of the entanglement contour. Making use of non-perturbative variational techniques based on fermionic Gaussian states, we have examined the spatio-temporal causal structure in the spread of entanglement carried by the produced particle-antiparticle pairs, and how the system can thermalise when looking at reduced parts. Our study reveals how the entanglement contour captures key phenomena, such as the cosmological particle horizon in a de Sitter spacetime, and how the effects of symmetry-breaking processes become very transparent when resolving the symmetries of the entanglement contour. Our work paves the way for future studies exploring further non-perturbative effects in interacting cQFTs, and encourages experimental efforts in Raman optical lattices to connect to these gravitational analogues.

Acknowledgements.— We acknowledge support from PID2021- 127726NB- I00 (MCIU/AEI/FEDER, UE), from the Grant IFT Centro de Excelencia Severo Ochoa CEX2020-001007-S, funded by MCIN/AEI/10.13039/501100011033, from the the CAM/FEDER Project TEC-2024/COM 84 QUITEMAD-CM, and from the CSIC Research Platform on Quantum Technologies PTI- 001.

* carlos.fulgado@estudiante.uam.es

- [1] R. P. Feynman, International journal of theoretical physics **21**, 467 (1982).
- [2] J. I. Cirac and P. Zoller, Nature Physics **8**, 264 (2012).
- [3] I. Georgescu, S. Ashhab, and F. Nori, Reviews of Modern Physics **86**, 153–185 (2014).
- [4] N. D. Birrell and P. C. W. Davies, *Quantum Fields in Curved Space*, Cambridge Monographs on Mathematical Physics (Cambridge Univ. Press, Cambridge, UK, 1984).
- [5] L. E. Parker and D. Toms, *Quantum Field Theory in Curved Spacetime: Quantized Field and Gravity*, Cambridge Monographs on Mathematical Physics (Cambridge University Press, 2009).
- [6] L. J. Garay, J. R. Anglin, J. I. Cirac, and P. Zoller, Phys. Rev. Lett. **85**, 4643 (2000).
- [7] U. R. Fischer and R. Schützhold, Phys. Rev. A **70**, 063615 (2004).
- [8] C. Barceló, S. Liberati, and M. Visser, Living Reviews in Relativity **8** (2005), 10.12942/lrr-2005-12.
- [9] R. Schutzhold, M. Uhlmann, L. Petersen, H. Schmitz, A. Friedenauer, and T. Schatz, Phys. Rev. Lett. **99**, 201301 (2007), arXiv:0705.3755 [quant-ph].
- [10] B. Horstmann, B. Reznik, S. Fagnocchi, and J. I. Cirac, Phys. Rev. Lett. **104**, 250403 (2010), arXiv:0904.4801 [quant-ph].
- [11] O. Lahav, A. Itah, A. Blumkin, C. Gordon, S. Rinott, A. Zayats, and J. Steinhauer, Physical Review Letters **105** (2010), 10.1103/physrevlett.105.240401.
- [12] S. Weinfurter, E. W. Tedford, M. C. J. Penrice, W. G. Unruh, and G. A. Lawrence, Physical Review Letters **106** (2011), 10.1103/physrevlett.106.021302.
- [13] J. Hu, L. Feng, Z. Zhang, and C. Chin, Nature Physics **15**, 785 (2019).
- [14] V. I. Kolobov, K. Golubkov, J. R. Muñoz de Nova, and J. Steinhauer, Nature Physics **17**, 362–367 (2021).
- [15] C. Viermann, M. Sparr, N. Liebster, M. Hans, E. Kath, A. Parra-López, M. Tolosa-Simeón, N. Sánchez-Kuntz, T. Haas, H. Strobel, S. Floerchinger, and M. K. Oberthaler, Nature **611**, 260–264 (2022).
- [16] P. Švančara, P. Smanioto, L. Solidoro, J. F. MacDonald, S. Patrick, R. Gregory, C. F. Barengi, and S. Weinfurter, Nature **628**, 66–70 (2024).
- [17] N. Laflorencie, Physics Reports **646**, 1–59 (2016).
- [18] P. Calabrese and J. Cardy, Journal of Statistical Mechanics: Theory and Experiment **2004**, P06002 (2004).
- [19] P. Calabrese and J. Cardy, Journal of Physics A: Mathematical and Theoretical **42**, 504005 (2009).
- [20] L. Zhang and X.-J. Liu, “Spin-orbit coupling and topological phases for ultracold atoms,” in *Synthetic Spin-Orbit Coupling in Cold Atoms*, Chap. Chapter 1, pp. 1–87.
- [21] X.-J. Liu, Z.-X. Liu, and M. Cheng, Phys. Rev. Lett. **110**, 076401 (2013).
- [22] X.-J. Liu, K. T. Law, and T. K. Ng, Phys. Rev. Lett. **112**, 086401 (2014).
- [23] X.-J. Liu, K. T. Law, and T. K. Ng, Phys. Rev. Lett. **113**, 059901 (2014).
- [24] Z. Wu, L. Zhang, W. Sun, X.-T. Xu, B.-Z. Wang, S.-C. Ji, Y. Deng, S. Chen, X.-J. Liu, and J.-W. Pan, Science **354**, 83 (2016).
- [25] W. Sun, B.-Z. Wang, X.-T. Xu, C.-R. Yi, L. Zhang, Z. Wu, Y. Deng, X.-J. Liu, S. Chen, and J.-W. Pan, Phys. Rev. Lett. **121**, 150401 (2018).
- [26] B. Song, L. Zhang, C. He, T. F. J. Poon, E. Hajiyeve, S. Zhang, X.-J. Liu, and G.-B. Jo, Science Advances **4** (2018).
- [27] M.-C. Liang, Y.-D. Wei, L. Zhang, X.-J. Wang, H. Zhang, W.-W. Wang, W. Qi, X.-J. Liu, and X. Zhang, Phys. Rev. Res. **5**,

L012006 (2023).

- [28] Y. Chen and G. Vidal, *Journal of Statistical Mechanics: Theory and Experiment* **2014**, P10011 (2014).
- [29] C. V. Kraus, M. M. Wolf, J. I. Cirac, and G. Giedke, *Phys. Rev. A* **79**, 012306 (2009).
- [30] C. V. Kraus and J. I. Cirac, *New Journal of Physics* **12**, 113004 (2010).
- [31] M. J. Jacquet, S. Weinfurter, and F. König, *Philosophical Transactions of the Royal Society A: Mathematical, Physical and Engineering Sciences* **378**, 20190239 (2020).
- [32] S. Dodelson, *Modern Cosmology* (Academic Press, Elsevier Science, 2003).
- [33] C. Fulgado-Claudio, J. M. S. Velázquez, and A. Bermudez, *Quantum* **7**, 1042 (2023).
- [34] K. G. Wilson, *Phys. Rev. D* **10**, 2445 (1974).
- [35] J. G. Valatin, *Il Nuovo Cimento* **7**, 843 (1958).
- [36] N. N. Bogolyubov, *Il Nuovo Cimento* **7**, 794 (1958).
- [37] D. J. Gross and A. Neveu, *Phys. Rev. D* **10**, 3235 (1974).
- [38] C. Fulgado-Claudio, P. Sala, D. González-Cuadra, and A. Bermudez, “Interacting dirac fields in an expanding universe: dynamical condensates and particle production,” (2024), arXiv:2408.06405 [gr-qc].
- [39] A. Bermudez, E. Tirrito, M. Rizzi, M. Lewenstein, and S. Hands, *Annals of Physics* **399**, 149 (2018).
- [40] J. L. Ball, I. Fuentes-Schuller, and F. P. Schuller, *Physics Letters A* **359**, 550 (2006).
- [41] S.-Y. Lin, C.-H. Chou, and B. L. Hu, *Phys. Rev. D* **81**, 084018 (2010).
- [42] I. Fuentes, R. B. Mann, E. Mart’ın-Mart’ınez, and S. Moradi, *Physical Review D* **82** (2010), 10.1103/physrevd.82.045030.
- [43] E. Mart’ın-Mart’ınez and N. C. Menicucci, *Classical and Quantum Gravity* **31**, 214001 (2014).
- [44] P. Calabrese and J. Cardy, *Journal of Statistical Mechanics: Theory and Experiment* **2005**, P04010 (2005).
- [45] M. Fagotti and P. Calabrese, *Physical Review A* **78** (2008), 10.1103/physreva.78.010306.
- [46] V. Alba and P. Calabrese, *Proceedings of the National Academy of Sciences* **114**, 7947–7951 (2017).
- [47] V. Alba and P. Calabrese, *SciPost Physics* **4** (2018), 10.21468/scipostphys.4.3.017.
- [48] B. Bertini, M. Fagotti, L. Piroli, and P. Calabrese, *Journal of Physics A: Mathematical and Theoretical* **51**, 39LT01 (2018).
- [49] V. Alba, B. Bertini, M. Fagotti, L. Piroli, and P. Ruggiero, *Journal of Statistical Mechanics: Theory and Experiment* **2021**, 114004 (2021).
- [50] S. N. Santalla, G. Ram’ırez, S. S. Roy, G. Sierra, and J. Rodríguez-Laguna, *Physical Review B* **107** (2023), 10.1103/physrevb.107.112114.
- [51] I. Peschel, *Journal of Physics A: Mathematical and General* **36**, L205 (2003).
- [52] J. Surace and L. Tagliacozzo, *SciPost Physics Lecture Notes* (2022), 10.21468/scipostphyslectnotes.54.
- [53] See Supplemental Material at URL-will-be-inserted-by-publisher.
- [54] J. M. Deutsch, *Phys. Rev. A* **43**, 2046 (1991).
- [55] M. Srednicki, *Physical Review E* **50**, 888–901 (1994).
- [56] J. M. Deutsch, *Reports on Progress in Physics* **81**, 082001 (2018).
- [57] L. Vidmar and M. Rigol, *Journal of Statistical Mechanics: Theory and Experiment* **2016**, 064007 (2016).
- [58] To ensure significant propagation since the beginning of the expansion, we impose an initial state with matter content. This is achieved via a quantum quench in the mass before the start of the expansion. Other alternatives to design the initial state

would lead to similar interplay with the horizon.

- [59] S. Ryu, A. P. Schnyder, A. Furusaki, and A. W. W. Ludwig, *New Journal of Physics* **12**, 065010 (2010).
- [60] C.-K. Chiu, J. C. Teo, A. P. Schnyder, and S. Ryu, *Reviews of Modern Physics* **88** (2016), 10.1103/revmodphys.88.035005.
- [61] A. W. W. Ludwig, *Physica Scripta* **T168**, 014001 (2015).
- [62] M. D. Schwartz, *Quantum Field Theory and the Standard Model* (Cambridge University Press, 2013).

SUPPLEMENTAL MATERIAL

Quasi-particle picture of entanglement spread

Here, we review the quasi-particle picture for the entanglement entropy, and extend it to the entanglement contour addressing how it gets affected by the presence of self-interactions of the Dirac fermions.

In its original realm, the quasi-particle picture describes the evolution of entanglement entropy as carried by propagating quasi-particles produced in pairs after a quantum quench. It was first introduced as a qualitative explanation for homogeneous quantum quenches in quantum chains [44], and then quantitatively demonstrated for the XY model [45] and other generic integrable models [46, 47]. It has also been studied for other entanglement measurements beyond entanglement entropy, such as the so-called entanglement links [50]. This picture suggests that, after a quantum quench, the initial state acts as a reservoir of excited quasi-particles that are created in pairs and propagate in straight lines with opposite velocities given by $v_k = \pm |\partial_k \epsilon_k|$, where ϵ_k is an energy dispersion relation for the quasi-particle labelled by k . From this perspective, when the system is partitioned into two spatial regions A and B , entanglement growth is due to entangled pairs of propagating quasi-particles residing in different sides of the partition. In our context of conformal time, the evolution of the EE can be thus expressed as

$$S_A(\eta) = \eta \int_{v_k > \frac{\ell_A}{2\eta}} \frac{dk}{2\pi} 2v_k s(k) + \ell_A \int_{v_k < \frac{\ell_A}{2\eta}} \frac{dk}{2\pi} s(k), \quad (5)$$

where the first term describes an initial linear increase of entanglement over conformal time, which accounts for a phase in which a quasiparticles are only entering in the A block. The second term, on the other hand, describes an equilibration to an extensive amount of entanglement proportional to ℓ_A that appears for sufficiently long times, such that the same amount of quasi-particles enter as those that exit the block. Note that, if there is a maximum propagation velocity, the limits of the integrals define an effective causal cone for the spread of entanglement in the system. In this formula, $s(k)$ denotes the amount of entanglement carried by the pair of quasi-particles, and can be obtained by analyzing the long-time behavior of the quantum state, which is expected to approach a generalised Gibbs ensemble (GGE) [49] with a well known thermodynamic entropy, or *ab initio* for certain type of integrable systems by knowing the specific form of the initial squeezed state [48].

In the scenario of cosmological Dirac fermions, these quasi-particles are described, after a antiparticle-hole transformation [62], as pairs of particles and antiparticles created back-to-back with opposite quasi-momentum, as described by Eq. (4) of the main text. For this case, closed formulas can be found for the mode entanglement between particles and antiparticles, which are derived by tracing out the sector of antiparticles from the density matrix. We have

$$\rho = \bigotimes_k \rho_k = \bigotimes_k (|\alpha_k|^2 |0\rangle\langle 0| + |\beta_k|^2 |1_k, \bar{1}_{-k}\rangle\langle 1_k, \bar{1}_{-k}|), \quad (6)$$

where we have defined $|1_k, \bar{1}_{-k}\rangle = \hat{a}_k^\dagger \hat{b}_{-k}^\dagger |0\rangle$. Then, tracing out the antiparticles sector, we arrive at

$$\rho_k^{\text{part}} = |\alpha_k|^2 |0\rangle\langle 0| + |\beta_k|^2 |1_k\rangle\langle 1_k|. \quad (7)$$

The entanglement entropy between particles and antiparticles in the mode k is therefore given by the von Neumann entropy of ρ_k^{part} , $S(\rho_k^{\text{part}}) = -\text{Tr}(\rho_k^{\text{part}} \log \rho_k^{\text{part}})$, which in terms of the Bogoliubov coefficients is given by

$$S(\rho_k^{\text{part}}) = -|\alpha_k|^2 \log |\alpha_k|^2 - |\beta_k|^2 \log |\beta_k|^2. \quad (8)$$

The relation between the Bogoliubov parameters for fermions, $|\alpha_k|^2 + |\beta_k|^2 = 1$, allows to construct this expression using only the spectrum of particle production, with entanglement entropy being upper-bounded by $S(\rho_k^{\text{part}}) \leq \log 2$ for $|\beta_k|^2 = \frac{1}{2}$. Using this expression, the contributions $s(k)$ in Eq. (5) are found to be $s(k) = 2S(\rho_k^{\text{part}})$, where the factor of 2 takes into account the two possibilities of a particle propagating out of the partition while an antiparticle stays inside and vice versa.

This quasi-particle prediction (5) is exact in the scaling limit $\ell_A, t \rightarrow \infty$, while keeping ℓ_A/t constant, and it gives the leading order contribution for large but finite t and ℓ_A for our propagating Dirac fields in the non-interacting limit $g_0^2 = 0$. In Fig. 4 we show the behavior of entanglement entropy evolution for two different values of ℓ_A . We observe some deviations for small times, but a good agreement with Eq. (5) for increasingly larger partition size as one approaches the scaling limit, according to the expected result.

We can now extend the quasi-particle prediction to the EC, which would yield the leading order contribution to the numerical results shown in Fig. 1 of the main text. The intuition behind it is that pairs of particle-antiparticle are created homogeneously along the partition. Those created at sites closer to the edges will contribute earlier to the increase of entanglement, and effectively one sees entanglement stemming from both boundaries with a maximum velocity given by $2v_{\text{max}} = 2\max_{k \in \text{BZ}} v_k$. This leads directly to the causal cones for entanglement displayed in that figure. The factor of 2 simply manifests the fact that both quasi-particles travel oppositely with the same velocity, so entanglement effectively travels at twice the speed of the individual quasi-particles. This behavior is captured by the following expression

$$S_A(\mathbf{x}) = \int \frac{dk}{2\pi} s(k) (\Theta(2v_k \eta - \mathbf{x}) + \Theta(2v_k \eta - (\ell_A - \mathbf{x}))), \quad (9)$$

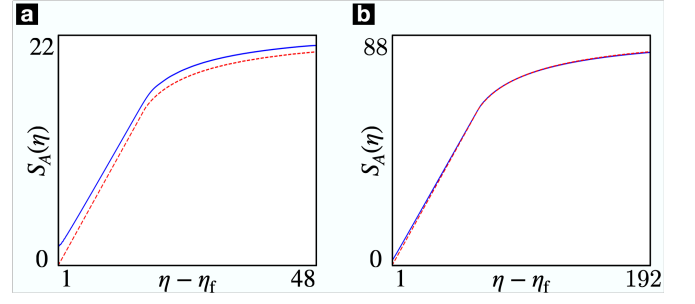


FIG. 4. Time evolution of entanglement entropy $S_A(\eta)$ for a partition of (a) $\ell_A = 32$ sites from a $N_S = 128$ sites system, and (b) $\ell_A = 128$ sites from a $N_S = 512$ sites system. The blue line represents the numerical result while the red dashed line represents the quasi-particle prediction. The parameters are set as $ma = 1$, $g_0^2 = 0$, $a_0 = 0.01$ and $a_f = 10$.

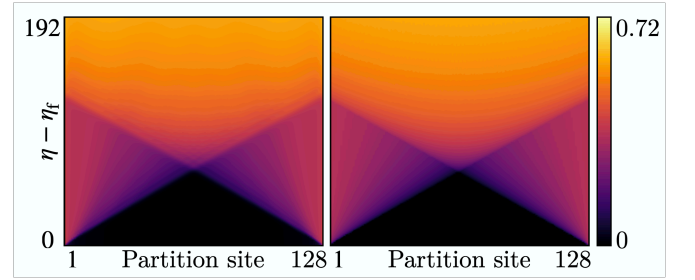


FIG. 5. Time evolution of entanglement contour $S_i(\eta)$ for a partition of $\ell_A = 128$ sites from a $N_S = 512$ sites system. The parameters are set as $ma = 1$, $g_0^2 = 0$, $a_0 = 0.01$ and $a_f = 10$. The left panel represents the numerical result, while the right panel represents the quasi-particle prediction according to Eq. (9).

where $\Theta(x)$ is the Heaviside step function. This picture translates naturally to our lattice field theory as, by virtue of the particle-hole symmetry, EC is enforced to be invariant upon the exchange of the spinor components, such that Eq. (9) distributes evenly between them, $S_A(\mathbf{x}, \alpha) = \frac{1}{2} S_A(\mathbf{x})$ for $\alpha \in \{u, d\}$. The comparison between the numerical computation and the quasiparticle prediction is shown in Fig. 5, showing a very clear agreement. The black region represents a causally-disconnected region of spacetime that shrinks as time goes by and excitations enter the block from the block complement B . When the two effective light-cones that emanate from the boundaries of the block meet, the whole A subsystem gets effectively entangled with B . This entanglement keeps on evolving until each cone reached the opposite boundary, such that the same number of excitations that enter leave A , and the subsystem equilibrates. It is interesting to see that the EC at this timescale becomes uniform across the block $S_i(\eta) \approx S_0$, such that the block EE equilibrates to a volume law $S_A = S_0 \ell_A$.

Now, we turn to the interacting regime. Within our variational fGS approach, interactions introduce a pair of self-consistent condensates into the dynamical Hamiltonian. After performing a quantum quench, these condensates are out-of-equilibrium and display a non-trivial evolution that modifies

both the number of produced particles and their propagation velocity. Therefore, the number of particles and antiparticles for each mode is no longer a constant of motion, and one may find deviations from the quasi-particle picture. We now discuss the specific changes that arise, and argue that in a certain parameter regime and for sufficiently long times, the quasi-particle picture can be minimally modified so that it still captures the essence of the entanglement spread.

First, we consider expansions with a vanishing pseudo-scalar condensate. In this case, the effect of interactions is to generate a scalar condensate that shifts the mass of the system, $m \rightarrow m + \Sigma(\eta)$. We find that, after a sudden period of exponential expansion $a_0 \rightarrow a_f$, the condensate displays some oscillations, after which it equilibrates to a certain non-zero value. Initially, the instantaneous velocity and number of particles oscillate, but eventually they also equilibrate, leading to a scaling limit in which the quasi-particle picture prediction in Eq. (9) is recovered by just replacing $s(k)$ by its equilibrium values, as shown in Fig. 6(a). The quasi-particle description is therefore valid in this interacting regime due to the presence of an equilibration process. The initial oscillations can be then understood as a finite-duration quench, after which the Hamiltonian renormalised by the self-energy equilibrates becoming static, and one can find constants of motion and recover the quasi-particle picture. It is noteworthy that, due to the finite size of the system, some revivals are observed after the equilibration for $\eta \approx \frac{N_s}{2}$, and one has to numerically check the suitability of the quasi-particle picture by comparing the time scales of relaxation of $\Sigma(\eta)$, which is determined by the self-consistent time-evolution governed by Eq. (3), and the time scales that one is able to explore numerically for a given system size.

On the other hand, when we consider expansions with a non-vanishing pseudo-scalar condensate $\Pi \neq 0$, the condensates display some synchronized and persistent oscillations that do not equilibrate for the time scales that we have explored (see Fig. 6(b)), and might connect to some long-wavelength hydrodynamic modes present at least in our fGS formalism. This leads to a long-lived oscillations of the number of particles and velocities of propagation. The lack of relaxation in this case restricts the applicability of Eq. (5), as shown in Fig. 6(c), where we show that any attempt to fix $s(k)$ by their later time values leads to a completely incorrect prediction. Additionally, we observe an oscillating pattern in the evolution of entanglement that emerges due to these persistent oscillations. With respect to EC, the same limitations apply, with Eq. (9) not being an accurate description of its numerical time-evolution. Additionally, in this case the spinor distribution of entanglement becomes non-trivial, yielding an interesting interplay with symmetry breaking as discussed in the main text, and which is not predicted either by the quasi-particle picture.

However, the EC evolution in Fig. 6(c) shows that the causal structure of the free case is not drastically modified, and by virtue of a maximal velocity of propagation $v^{\max} = \max_{k \in \text{BZ}} v_k(\eta)$ a causal cone $x(\eta) = \int^\eta v^{\max}(\eta') d\eta'$ can still

be defined in the interacting regime, settling a boundary to entanglement spreading (white lines). In these cones, the oscillations of the condensates are also explicit, but they act only as a small perturbation to the linear propagation. This, combined with the imbalance of entanglement between both legs, permits to bound the spatial propagation of EC, connecting with the description of causal cones of entanglement while allowing to probe spontaneous symmetry breaking of discrete symmetries, as discussed in the main text.

Parity-breaking spectra and time-reversal symmetry

Here, we show how the persistence of a symmetric spectrum of production in the quench limit for parity-breaking expansions follows from the persistence of time-reversal symmetry. As discussed in the main text, the Hamiltonian that governs time-evolution within our variational fermionic Gaussian state (fGS) ansatz is

$$\tilde{h}_k(ma(\eta)) = -\frac{\sin ka}{a} \gamma^0 \gamma^1 + \left(ma(\eta) + \Sigma + \frac{1 - \cos ka}{a} \right) \gamma^0 - i\Pi \gamma^1, \quad (10)$$

where $\Sigma = g_0^2 \sum_k \langle \hat{\psi}_k^\dagger \gamma^0 \hat{\psi}_k \rangle / 2aN_s$, $\Pi = ig_0^2 \sum_k \langle \hat{\psi}_k^\dagger \gamma^1 \hat{\psi}_k \rangle / 2aN_s$ are respectively the scalar and pseudo-scalar fermion condensates. For values of the parameters for which $\Pi \neq 0$, parity, particle-hole and sub-lattice symmetries are broken. Additionally, when considering an expanding universe with a time-dependent scale factor $a(\eta)$, the remaining time-reversal symmetry must be analyzed more carefully. First, one must select a specific value of time with respect to which the time reflection is performed. In our case, it is sensible to choose the initial time of the expansion η_0 . Then, one finds that the condition for a Hamiltonian to be symmetric under time reversal becomes $T^\dagger h_{-k}^*(\eta) T = h_k(2\eta_0 - \eta)$. Clearly, the single-particle Hamiltonian in Eq. (10) with the scale factor under consideration does not respect this symmetry, as the expansion imposes a unique direction of time. However, the above condition is fulfilled instantaneously for $\eta = \eta_0$, so the properties that time-reversal imposes over the different observables are realised at $\eta = \eta_0$ and they disappear for $\eta > \eta_0$. Regarding the effect of these symmetries, while both parity and time-reversal transformations connect operators with opposite quasi-momenta, $\hat{P} \hat{\psi}_k \hat{P}^{-1} = \hat{T} \hat{\psi}_k \hat{T}^{-1} = \gamma^0 \hat{\psi}_{-k}$, only parity relates modes connected through a spatial reflection, $\hat{P} \hat{\psi}_i \hat{P}^{-1} = \gamma^0 \hat{\psi}_{N_s+1-i} = \hat{T} \hat{\psi}_{N_s+1-i} \hat{T}^{-1}$. This manifests that \hat{P} is a unitary operator, while \hat{T} is anti-unitary. It is precisely these properties of time-reversal that underlies the results found in Figs. 2-3 of the main text, which suggest the presence of a transformation that reflects quasi-momentum while leaving real space unaltered. Let us therefore explain the aforementioned results using the notion of time-reversal symmetry in this context.

While parity is broken for expansions within the Aoki phase, time-reversal still plays a role at $\eta = \eta_0$. Since the in-

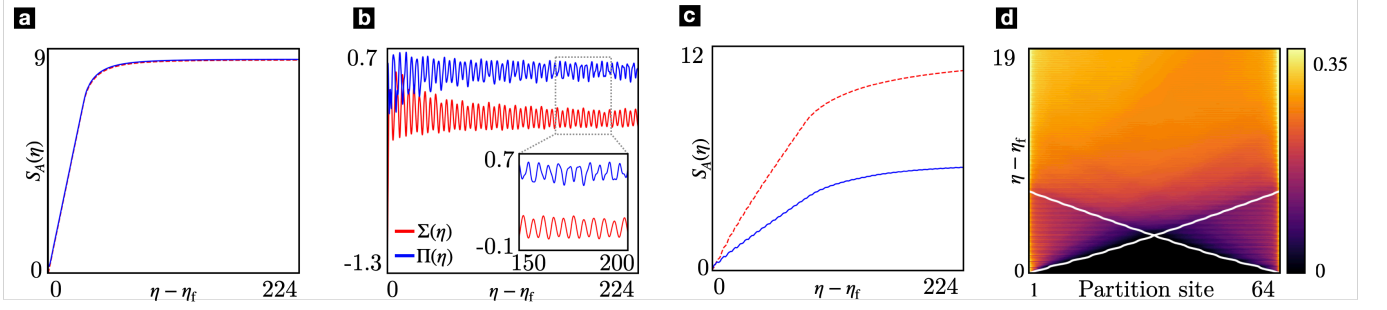


FIG. 6. **(a)** Evolution of entanglement entropy of a $\ell_A = 64$ partition of a $N_S = 512$ sites system after an expansion with a vanishing pseudo-scalar condensate $\Pi = 0$. The blue line represents the numerical result while the red dashed line represents the quasi-particle prediction. The parameters are set as $ma = 1$, $a_0 = 0.01$, $a_f = 10$, $g_0^2 = 3$ and $Ha = 100$. **(b)** Evolution of the scalar and pseudo-scalar condensates for a system of $N_S = 512$ sites, showing their persistent oscillating behavior. The parameters are set as $ma = -1$, $a_0 = 0.7$, $a_f = 1.3$, $g_0^2 = 3$ and $Ha = 100$. **(c)** Evolution of entanglement entropy of a $\ell_A = 64$ partition of a $N_S = 512$ sites system after an expansion with both a non-vanishing scalar and pseudo-scalar condensates, $\Sigma, \Pi \neq 0$. The blue line represents the numerical result while the red dashed line represents the quasi-particle prediction. The parameters are the same as in **(b)**. **(d)** Evolution of entanglement contour of a $\ell_A = 64$ partition of a $N_S = 512$ sites system after an expansion with both a non-vanishing scalar and pseudo-scalar condensates, $\Sigma, \Pi \neq 0$. We show the contribution from the upper component of the spinor field to the EC, S_i^u . The white lines correspond to the curves $x(\eta) = \int_{\eta_f}^{\eta} v_g(\eta') d\eta'$. The parameters are the same as in **(b)**.

stantaneous Hamiltonian $\hat{H}(\eta_0)$ fulfills the time-reversal symmetry criterion, its groundstate $|\text{gs}_0\rangle$ is time-reversal symmetric. As a consequence, when computing the density of produced particles, one finds that

$$\begin{aligned}
 |\beta_k|^2 &= \langle \text{gs}_0 | \hat{a}_k^\dagger \hat{a}_k | \text{gs}_0 \rangle \\
 &= \langle \text{gs}_0 | \hat{T}^\dagger \hat{T} \hat{a}_k^\dagger \hat{T}^{-1} \hat{T} \hat{a}_k \hat{T}^{-1} \hat{T} | \text{gs}_0 \rangle^* = \\
 &= \langle \text{gs}_0 | \hat{a}_{-k}^\dagger \hat{a}_{-k} | \text{gs}_0 \rangle = |\beta_{-k}|^2,
 \end{aligned} \tag{11}$$

even when parity no longer protects this symmetry. On the other hand, when the value of Ha decreases and the expansion slows down, particle production is no longer computed over the initial groundstate $|\text{gs}_0\rangle$, but over the evolved state given by Eq. (4). Since this state has evolved under the full time-dependent Hamiltonian which is consequently not time-reversal invariant, the above result is no longer fulfilled, leading to the asymmetric spectra in Fig. 3 for small values of Ha .